PROCEEDINGS A

rspa.royalsocietypublishing.org

Research

Article submitted to journal

Subject Areas:
Applied Mathematics

Keywords:
Eigenvalues, Bi-Laplacian, Singular Perturbations

Author for correspondence:
A. E. Lindsay
e-mail: a.lindsay@nd.edu

Vibrations of thin plates with small clamped patches.

A. E. Lindsay[1], W. Hao[2] and A. J. Sommese[1]

[1]Dept. of Applied and Computational Math and Statistics, University of Notre Dame, IN, 46617, USA.
[2]Mathematical BioSciences Institute, Ohio State University, 380 Jennings Hall, OH, 43210, USA.

Eigenvalues of fourth order elliptic operators feature prominently in stability analysis of elastic structures. This paper considers out-of-plane modes of vibration of a thin elastic plate perforated by a collection of small clamped patches. As the radius of each patch shrinks to zero, a *point constraint eigenvalue problem* is derived in which each patch is replaced by a homogeneous Dirichlet condition at its center. The limiting problem is consequently not the eigenvalue problem with no patches, but a new type of spectral problem. The discrepancy between the eigenvalues of the patch free and point constraint problems are calculated. The dependence of the point constraint eigenvalues on the location(s) of clamping is studied numerically using techniques from numerical algebraic geometry. The vibrational frequencies are found to depend very sensitively on the number and center(s) of the clamped patches. For a range of number of punctures, we find spatial clamping patterns which correspond to local maxima of the base vibrational frequency of the plate.

THE ROYAL SOCIETY PUBLISHING

1. Introduction

Determining the spectra of fourth order elliptic operators is a ubiquitous problem arising in structural analysis of rigid objects. Two central problems (cf. [34]) are the determination of modes of vibration u of a thin plate $\Omega \subset \mathbb{R}^2$ satisfying

$$\Delta^2 u = \lambda u, \qquad \mathbf{x} \in \Omega, \tag{1.1a}$$

and the plate buckling problem

$$\Delta^2 u = \lambda \Delta u, \qquad \mathbf{x} \in \Omega. \tag{1.1b}$$

where $\Delta \equiv \partial_{xx}^2 + \partial_{yy}^2$ is the standard Laplacian. In each case, the goal is to determine, either analytically or numerically, the scalar eigenvalues λ_k and the corresponding eigenfunctions $u_k(\mathbf{x})$ satisfying (1.1). The governing equations (1.1) are supplemented with boundary conditions which vary with particular applications. A common assumption is the clamped condition

$$u = \frac{\partial u}{\partial n} = 0, \qquad \mathbf{x} \in \partial\Omega, \tag{1.1c}$$

which stipulates zero deflection and gradient of deflection on the periphery of the plate. In many engineering systems, such as heat exchangers [28,32,37], porous elastic materials and acoustic tiling [3,25,38], the elastic structure is not homogeneous but features a configuration of perforations. The incorporation of these perforations allows for manipulation of acoustic and vibrational properties of the plate while realizing economies from weight reductions and material costs. In cases where the pattern of perforation is periodic, homogenization theories can be applied to replace the plate's natural elastic modulus with an effective modulus [2,9]. However, this averaging approach does not provide detailed information of the dependence of the modes on particular perforation locations.

The perforation structure, denoted Ω_ε, can be formally defined as a collection of small patches of common radius ε and written explicitly as

$$\Omega_\varepsilon = \bigcup_{k=1}^{N} (\mathbf{x}_k + \varepsilon\, \Omega_k), \tag{1.2}$$

where the patch centers are given by $\{\mathbf{x}_k\}_{k=1}^N$ and each patch may have its own particular non-circular geometry Ω_k. The plate itself then occupies the domain $\Omega \setminus \Omega_\varepsilon$ (cf. Fig. 1).

The problem considered in the present work is the determination of the free modes of vibration (solutions to (1.1*a*)) in the presence of the perforation structure (1.2). This leads to consideration of the fourth order partial differential equation (PDE)

$$\Delta^2 u_\varepsilon = \lambda_\varepsilon u_\varepsilon\,, \quad \mathbf{x} \in \Omega \setminus \Omega_\varepsilon\,; \quad \int_{\Omega\setminus\Omega_\varepsilon} u_\varepsilon^2 \,\mathrm{d}\mathbf{x} = 1; \tag{1.3a}$$

$$u_\varepsilon = \frac{\partial u_\varepsilon}{\partial n} = 0\,, \quad \mathbf{x} \in \partial\Omega_\varepsilon\,; \quad u_\varepsilon = \frac{\partial u_\varepsilon}{\partial n} = 0, \quad \mathbf{x} \in \partial\Omega, \tag{1.3b}$$

where $\Omega \setminus \Omega_\varepsilon$ is the extent of the plate and Ω_ε is the collection of patches. Clamped boundary conditions (1.3*b*) are applied to the periphery of the domain and on each perturbing perforation.

The focus of the present work is to study the dependence of the eigenvalues λ_ε on Ω_ε, and more specifically on the number N and locations $\{\mathbf{x}_k\}_{k=1}^N$ of the perturbing patches, in the limit $\varepsilon \to 0$.

Before detailing the main results of this study, it is useful to review established key results. A good deal of mathematical interest in the bi-Laplacian eigenvalue problem has focussed on the qualitatively different behaviors of (1.3) compared to its well understood second order elliptic counterpart. A key property of problem (1.3) is that the fundamental eigenfunction, ie. that associated with the lowest eigenvalue, is not guaranteed to be of one sign [12–14,18,20,35]. This contrasts sharply with classical results for the eigenvalue problem for the Laplacian [15,19]. In the case of the annular region $\varepsilon < r < 1$, detailed properties of Bessel functions [13] determine that for

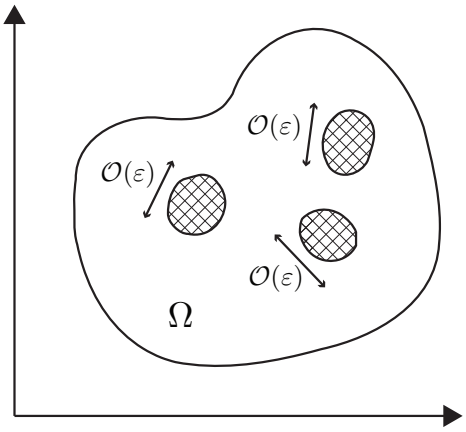

Figure 1. Schematic of a domain Ω representing the extent of a plate with three small clamped patches of radius $\mathcal{O}(\varepsilon)$.

$\varepsilon^{-1} > 762.36$, the fundamental eigenvalue is not simple and the corresponding eigenspace is two-dimensional. In domains with a corner, the first eigenfunction may possess an infinite number of nodal lines [12]. The numerical treatment of fourth order eigenvalue problems, with and without perforations, requires careful attention to account for these complexities and has led to many specialized methodologies [1,8,11,26,30].

There are additional remarkable phenomena associated with the bi-Laplacian eigenvalue problem in domains with small subdomains removed. One may expect that as $\varepsilon \to 0$, $(u_\varepsilon, \lambda_\varepsilon)$ would approach $(u^\star, \lambda^\star)$, the problem with no patches satisfying

$$\Delta^2 u^\star = \lambda^\star u^\star\,, \quad \mathbf{x} \in \Omega\,; \qquad u^\star = \frac{\partial u^\star}{\partial n} = 0\,, \quad \mathbf{x} \in \partial\Omega; \qquad \int_\Omega u^{\star 2}\,\mathrm{d}\mathbf{x} = 1. \tag{1.4}$$

However, such limiting behavior is atypical. In the case where a single circular subdomain of radius ε and centered at $\mathbf{x}_0$ is removed, the limiting behavior is $\lim_{\varepsilon\to 0} u_\varepsilon = u_0$ where u_0 is a distinct *point constraint eigenvalue problem*

$$\Delta^2 u_0 = \lambda_0 u_0, \quad \mathbf{x} \in \Omega; \qquad \int_\Omega u_0^2\,\mathrm{d}\mathbf{x} = 1; \tag{1.5a}$$

$$u_0 = \frac{\partial u_0}{\partial n} = 0, \quad \mathbf{x} \in \partial\Omega; \qquad u_0(\mathbf{x}_0) = 0. \tag{1.5b}$$

A comparison between (1.3*b*) and (1.5*b*) indicates that the clamped condition on the patch is retained in the limit as $\varepsilon \to 0$ through a point constraint $u_0(\mathbf{x}_0) = 0$ on the limiting eigenfunction. Note that the condition on the gradient of the eigenfunction is not retained. For the case of a single patch, the limiting behavior of the eigenvalues λ_ε of (1.3) was determined [10,29] to be

$$\lambda_\varepsilon = \lambda_0 + 4\pi\nu\,|\nabla u_0(\mathbf{x}_0)|^2 + \mathcal{O}(\nu^2), \qquad \nu = \frac{-1}{\log\varepsilon}, \tag{1.6}$$

as $\varepsilon \to 0$, provided $|\nabla u_0(\mathbf{x}_0)| \neq 0$. Higher order corrections to the behavior (1.6) were also calculated in [10,29] for both the case $|\nabla u_0(\mathbf{x}_0)| \neq 0$ and the degenerate scenario $|\nabla u_0(\mathbf{x}_0)| = 0$. In the exactly solvable case of the annular region $\varepsilon < r < 1$, this singular limiting behavior is manifested in a plot (cf. Fig. 2) of λ_ε against $\varepsilon \to 0$ as a jump discontinuity at $\varepsilon = 0$. In the case of a rectangular domain, numerical studies (cf. [16]) of (1.5) have found that a single puncture has a significant localizing effect on the eigenfunctions. Specifically, the presence of a puncture may subdivide Ω into distinct regions of high and low energy.

We remark that the limiting behavior of eigenvalues to (1.3) as $\varepsilon \to 0$ is qualitatively very different from the well established behavior of the eigenvalues of the Laplacian (cf. [17,27,33, 39,40]) in the presence of small perturbing holes. In such problems, the limiting behavior is to the

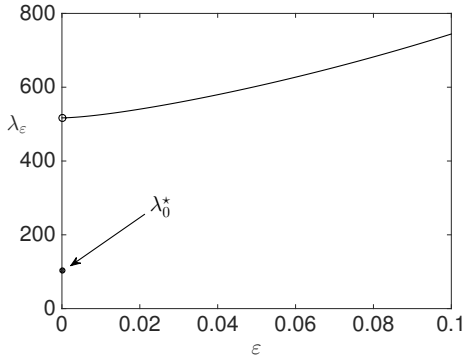

Figure 2. First eigenvalue associated with the radially symmetric eigenfunction of (1.3) on the annulus $\varepsilon < r < 1$. The lowest eigenvalue $\lambda_0^\star$ of the patch free problem (1.4) is indicated by an open circle on the vertical axis.

patch free problem. This dichotomy between limiting behaviors between the second and fourth order eigenvalue problems has recently been studied in a mixed order problem (cf. [31]).

In this paper, we consider problem (1.3) in the presence of N punctures and in the limit $\varepsilon \to 0$. In Sec. 2, we study a simplified model problem in the annulus $\varepsilon < r < 1$ with clamped boundary conditions. This serves to illustrate the discontinuous behavior of (1.3) as $\varepsilon \to 0$ in an exactly solvable situation. These reduced problems also serve as a guide for the analysis of the general case (1.3) where exact solutions are not available.

In Sec. 3, we analyze the limiting behavior of (1.3) as $\varepsilon \to 0$ and assuming the non-degeneracy condition $\sum_{k=1}^N |\nabla u_0(\mathbf{x}_k)|^2 \neq 0$, derive the limiting behavior

$$\lambda_\varepsilon = \lambda_0 + \sum_{k=1}^{\infty} \lambda_k \nu^k + \mathcal{O}(\mu), \qquad \nu = \frac{-1}{\log \varepsilon} \tag{1.7}$$

as $\varepsilon \to 0$ where $\mu = \mathcal{O}(\nu^M)$ for any integer M. The limiting point constraint problem for (u_0, λ_0) is

$$\Delta^2 u_0 = \lambda_0 u_0\,, \quad \mathbf{x} \in \Omega \setminus \{\mathbf{x}_k\}_{k=1}^N\,; \quad u_0 = \frac{\partial u_0}{\partial n} = 0\,, \quad \mathbf{x} \in \partial\Omega; \tag{1.8a}$$

$$\int_\Omega u_0^2 \,\mathrm{d}\mathbf{x} = 1; \qquad u_0(\mathbf{x}_k) = 0, \qquad k = 1, \ldots, N, \tag{1.8b}$$

and explicit formula are given for the correction terms λ_k in (3.13). The one term case is given by

$$\lambda_\varepsilon = \lambda_0 + 4\pi\nu \sum_{k=1}^{N} |\nabla u_0(\mathbf{x}_k)|^2 + \mathcal{O}(\nu^2), \qquad \nu = \frac{-1}{\log \varepsilon}, \tag{1.9}$$

as $\varepsilon \to 0$. In Sec. 3(a), an explicit expression for $\lambda^\star - \lambda_0$, the magnitude of the jump discontinuity (cf. Fig. 2) in λ_ε as $\varepsilon \to 0$ is derived. This deviation depends on the number and locations $\{\mathbf{x}_k\}_{k=1}^N$ of the patch centers.

In Sec. 4 we develop a numerical methodology to solve for the limiting eigenfunctions and eigenvalues and investigate the dependence of the eigenvalues on the configuration of centers $\{\mathbf{x}_k\}_{k=1}^N$ for a range of N. An analytical treatment of this question is challenging due to a lack of an explicit Green's function with which to express closed form solutions of (1.8). To overcome issues relating to high condition numbers, notorious in discretizations of fourth order partial differential equations, we employ the adaptive precision solver `Bertini` (cf. [4,5]). In particular, our numerical methodology allows us to determine particular arrangements of punctures $\{\mathbf{x}_k\}_{k=1}^N$ which maximize the first eigenvalue λ_0. For the range $N = 1, \ldots, 9$, we

determine (locally) optimal configurations of patch centers. In Sec. 5 we discuss future avenues of investigation which arise from this work.

2. A model problem with a point constraint

In this section, we consider the reduced model problem for the deflection of the annular plate $\varepsilon < r < 1$ under a load $f(\mathbf{x})$. The purpose of this example is to clarify the presence and consequences of a point constraint in the limiting problem in the simplest possible and exactly solvable setting. This also serves to highlight the phenomena that will appear in (1.3) and gives explicit information on the limiting form of solutions. The problem considered is the clamped plate under load

$$\Delta^2 u_\varepsilon = f, \qquad \varepsilon < r < 1, \quad 0 < \theta < 2\pi; \qquad u_\varepsilon = \frac{\partial u_\varepsilon}{\partial r} = 0, \quad \text{on} \quad r = 1, \text{ and } r = \varepsilon, \tag{2.1}$$

for symmetric and asymmetric loading functions f. This problem is simpler than the corresponding eigenvalue problem for annulus as there is no unknown λ to be determined. The eigenvalue problem for the annulus has been considered in [13] and some key results are reviewed later in Sec. 4.

(a) Case $f = 1$

In the case $\varepsilon = 0$ in which there is no perturbing patch, the solution of (2.1) is denoted $u^\star$ and the radially symmetric solution is calculated to be

$$u^\star(r) = \frac{1}{64}\Big(r^4 - 2r^2 + 1\Big). \tag{2.2}$$

We note that $u^\star(0) = 1/64$. In the case where $\varepsilon > 0$ and there is a circular patch of radius ε centered at the origin, the general solution of (2.1) satisfying the conditions at $r = 1$ is given by

$$u_\varepsilon = \frac{1}{64}\Big(r^4 - 1 + A_\varepsilon(r^2 - 1) - (4 + 2A_\varepsilon + B_\varepsilon)\log r + B_\varepsilon r^2 \log r\Big). \tag{2.3}$$

A system of equations for constants $\{A_\varepsilon, B_\varepsilon\}$ is determined by applying the boundary conditions at $r = \varepsilon$ and the limiting behavior as $\varepsilon \to 0$ is

$$A_\varepsilon = -1 + \varepsilon^2\big(-1 + \log\varepsilon + 4\log^2\varepsilon\big) + \mathcal{O}(\varepsilon^4 \log^4 \varepsilon),$$

$$B_\varepsilon = -2 + \varepsilon^2\big(-2 - 8\log\varepsilon - 8\log^2\varepsilon\big) + \mathcal{O}(\varepsilon^4 \log^4 \varepsilon).$$

This implies from (2.3) that

$$u_\varepsilon = \frac{1}{64}\Big(r^4 - r^2 - 2r^2\log r\Big) + \varepsilon^2\log^2\varepsilon\,\frac{1}{16}\Big(r^2 - 1 - 2r^2\log r\Big) + \mathcal{O}(\varepsilon^2\log\varepsilon), \tag{2.4}$$

which gives rise to the limiting function $u_0(r)$ satisfying

$$u_0(r) = \lim_{\varepsilon\to 0} u_\varepsilon = \frac{1}{64}\Big(r^4 - r^2 - 2r^2\log r\Big). \tag{2.5}$$

A comparison between (2.5) and the unperturbed solution $u^\star(r)$ of (2.2) shows that the limiting problem does not converge to the patch free problem, and in particular, $u_0(r)$ features the point constraints $u_0(0) = \partial_r u_0(0) = 0$. We also remark that the limiting function $u_0(r)$ is not smooth and satisfies $\Delta u_0 = \mathcal{O}(\log r)$ as $r \to 0$. The limiting form of (2.4) reveals that the expansion for u_ε of (2.1) in the case $f = 1$ is of form

$$u_\varepsilon = u_0 + \varepsilon^2\log^2\varepsilon\, u_1 + \varepsilon^2\log\varepsilon\, u_2 + \varepsilon^2 u_3 + \mathcal{O}(\varepsilon^4\log^4\varepsilon). \tag{2.6}$$

This particular example is a degenerate case due to the condition $\partial_r u_0(0) = 0$. To investigate the non-degenerate case $\partial_r u_0(0) \neq 0$, we consider an asymmetric forcing f.

(b) Case $f = \cos\theta$

In the absence of a patch ($\varepsilon = 0$), the smooth solution of problem (2.1) is

$$u^\star(r) = \frac{\cos\theta}{64}\Big(r^4 - \frac{3r^3}{2} + \frac{r}{2}\Big), \tag{2.7}$$

and in this case we notice that $u^\star(0) = 0$. As before, the annulus $\varepsilon < r < 1$ is considered and the limit $\varepsilon \to 0$ investigated. The problem (2.1) for $\varepsilon > 0$ has a general solution spanned by $\{\cos\theta\} \times \{r^3, r\log r, r, r^{-1}\}$. Incorporating the conditions at $r = 1$, gives

$$u_\varepsilon = \frac{\cos\theta}{64}\Big(r^4 + A_\varepsilon\, r^3 + B_\varepsilon\, r - (5 + 2B_\varepsilon + 4A_\varepsilon) r\log r - (1 + A_\varepsilon + B_\varepsilon)\,\frac{1}{r}\Big), \tag{2.8}$$

with $\{A_\varepsilon, B_\varepsilon\}$ determined by enforcing $u_\varepsilon = \partial_r u_\varepsilon = 0$ on $r = \varepsilon$. The limiting behavior of $\{A_\varepsilon, B_\varepsilon\}$ as $\varepsilon \to 0$ is

$$A_\varepsilon = \frac{5\nu - 6}{4(1-\nu)} + \mathcal{O}(\varepsilon^2\log\varepsilon), \qquad B_\varepsilon = \frac{2-\nu}{4(1-\nu)} + \mathcal{O}(\varepsilon^2\log\varepsilon), \qquad \nu = \frac{-1}{\log\varepsilon},$$

which takes the form of a geometric series in ν, a so called *logarithmic series*. The series can be expanded in ν to give

$$u_\varepsilon = \frac{\cos\theta}{64}\Big(r^4 - \frac{3r^3}{2} + \frac{r}{2}\Big) + \nu\, u_1 + \mathcal{O}(\nu^2), \tag{2.9}$$

In this example, $u_0(0) = 0$ and $u^\star = \lim_{\varepsilon\to 0} u_\varepsilon$ in accordance with intuitive expectation.

These model problems indicate two qualitative solution regimes that we can expect to encounter in the eigenvalue problem (1.3). First, in the case of a single clamping point $\mathbf{x}_0$, if $u^\star(\mathbf{x}_0) = 0$ then the limiting problem u_0 will coincide with the unperturbed problem. This result is encapsulated later in Theorem 3. The second is that we can expect two different type of expansions, depending wherever the gradient of the function at the clamping point $\nabla u_0(\mathbf{x}_0)$ is zero or not. In the non-degenerate scenario $\nabla u_0(\mathbf{x}_0) \neq 0$, the expansion is a logarithmic series, whereas if $\nabla u_0(\mathbf{x}_0) = 0$, the expansion is of form (2.6).

3. Derivation of the limiting behavior

In this section, we consider the eigenvalue problem (1.3) and determine the limiting behavior of a simple (multiplicity one) eigenpair $(u_\varepsilon, \lambda_\varepsilon)$ of (1.3) in the limit as $\varepsilon \to 0$. As motivated by the simplified example of the previous section, we will assume that the corresponding eigenfunction of the limiting point constraint problem satisfies a certain non-degeneracy condition.

To construct solutions of (1.3) in the limit as $\varepsilon \to 0$, we first note that $\Omega_\varepsilon \to \{\mathbf{x}_k\}_{k=1}^N$ as $\varepsilon \to 0$, which implies that the patch centered at $\mathbf{x}_k$ must be replaced by an equivalent local condition on the limiting eigenfunction as $\mathbf{x} \to \mathbf{x}_k$. To establish this condition at the k-th patch, we consider the rescaled problem in the stretched variables

$$\mathbf{y} = \varepsilon^{-1}(\mathbf{x} - \mathbf{x}_k)\,, \qquad v_k(\mathbf{y}) = u(\mathbf{x}_k + \varepsilon\mathbf{y})\,, \tag{3.1}$$

and introduce the vector valued canonical problem $v_k(\mathbf{y})$, satisfying

$$\Delta^2 v_k = 0\,, \qquad \mathbf{y} \in \mathbb{R}^2 \setminus \Omega_k\,; \qquad v_k = \frac{\partial v_k}{\partial n} = 0\,, \qquad \mathbf{y} \in \partial\Omega_k\,; \tag{3.2a}$$

$$v_k \sim \mathbf{y}\log|\mathbf{y}| + \mathcal{M}_k\mathbf{y} + \mathcal{O}(1)\,, \quad \text{as} \quad |\mathbf{y}| \to \infty\,. \tag{3.2b}$$

In (3.2*b*), the matrix $\mathcal{M}_k$ is determined by the shape of the patch Ω_k and can be identified explicitly in a few simple cases. When Ω_k is the unit disk, the exact solution of (3.2) is

$$v_k = \mathbf{y}\log|\mathbf{y}| - \frac{\mathbf{y}}{2} + \frac{\mathbf{y}}{2|\mathbf{y}|^2},$$

which corresponds to $\mathcal{M}_k = -I/2$ where I is the 2×2 identity matrix. In the example of an ellipse with semi-major axis a, semi-minor axis b for $a > b$ and where the semi-minor axis is inclined at

an angle α to the horizontal coordinate, the matrix entries of $\mathcal{M}_k$ are (cf. Appendix B of [36])

$$m_{11} = \frac{(b-a)\cos^2\alpha - b}{a+b} - \log\left(\frac{a+b}{2}\right), \qquad m_{22} = \frac{(a-b)\cos^2\alpha - a}{a+b} - \log\left(\frac{a+b}{2}\right),$$

$$m_{12} = m_{21} = -\frac{(a-b)\sin\alpha\cos\alpha}{a+b}.$$

For general Ω_k, $\mathcal{M}_k$ can be numerical computed by a boundary integral method (cf. Sec. 5 of [36]).

The logarithmic terms in the far field behavior (3.2*b*) of the canonical function v_k indicate that the inner solution v near $\mathbf{x} = \mathbf{x}_k$ should have an infinite series expansion in powers of $\nu(\varepsilon) = -1/\log\varepsilon$ of the form $v \sim \varepsilon\nu\sum_{m=0}^{\infty}(\mathbf{a}_{m,k}\cdot v_k)\nu^m$ where $\mathbf{a}_{m,k}$ are vector valued constants whose value will be determined. Upon using the far-field behavior (3.2*b*) in this infinite sum, and writing the resulting expression in the variable $(\mathbf{x}-\mathbf{x}_k)$ through (3.1), we obtain the matching condition

$$u(\mathbf{x}) \sim \mathbf{a}_{0,k}\cdot(\mathbf{x}-\mathbf{x}_k) + \sum_{m=1}^{\infty}\left[\mathbf{a}_{m-1,k}\cdot(\mathbf{x}-\mathbf{x}_k)\log|\mathbf{x}-\mathbf{x}_k| + (\mathbf{a}_{m-1,k}\cdot\mathcal{M}_k + \mathbf{a}_{m,k})\cdot(\mathbf{x}-\mathbf{x}_k)\right]\nu^m, \tag{3.3}$$

for the limiting eigenfunction as $\mathbf{x}\to\mathbf{x}_k$. The form of (3.3) suggests that the limiting eigenfunction for (1.3) should be expanded as

$$\lambda = \lambda_0 + \sum_{m=1}^{M}\nu^m\lambda_m + \mathcal{O}(\nu^{M+1}), \qquad u = u_0 + \sum_{m=1}^{M}\nu^m u_m + \mathcal{O}(\nu^{M+1}), \qquad \nu = \frac{-1}{\log\varepsilon},$$

for any integer M. Notice that the form of this asymptotic expansion corresponds to the model example of Sec. 2(b) in the non-degenerate case. Upon substituting this expansion into (1.3), we equate terms at each order of ν to obtain a sequence of problems. At leading order, the pair (λ_0, u_0) satisfies

$$\Delta^2 u_0 = \lambda_0 u_0, \quad \mathbf{x}\in\Omega\setminus\{\mathbf{x}_k\}_{k=1}^N, \quad u_0 = \frac{\partial u_0}{\partial n} = 0, \quad \mathbf{x}\in\partial\Omega; \qquad \int_\Omega u_0^2\,\mathrm{d}\mathbf{x} = 1; \tag{3.4a}$$

$$u_0 \sim \mathbf{a}_{0,k}\cdot(\mathbf{x}-\mathbf{x}_k) + \cdots, \quad \text{as} \quad \mathbf{x}\to\mathbf{x}_k, \qquad k = 1,\ldots,N. \tag{3.4b}$$

Matching (3.4*b*) with (3.3) at each $\mathbf{x} = \mathbf{x}_k$ then provides the conditions that

$$u_0(\mathbf{x}_k) = 0, \qquad \mathbf{a}_{0,k} = \nabla u_0|_{\mathbf{x}=\mathbf{x}_k}, \qquad k = 1,\ldots,N. \tag{3.4c}$$

The limiting eigenfunction $u_0(\mathbf{x})$ can be represented as

$$u_0(\mathbf{x}) = 8\pi\sum_{k=1}^{N}\alpha_k G(\mathbf{x};\mathbf{x}_k,\lambda_0), \tag{3.5}$$

where $G(\mathbf{x};\boldsymbol{\xi},\lambda)$ is the bi-Laplacian Helmholtz Green's function satisfying

$$-\Delta^2 G + \lambda G = -\delta(\mathbf{x}-\boldsymbol{\xi}), \quad \mathbf{x}\in\Omega; \qquad G = \frac{\partial G}{\partial n} = 0, \quad \mathbf{x}\in\partial\Omega; \tag{3.6a}$$

$$G(\mathbf{x};\boldsymbol{\xi},\lambda) = \frac{1}{8\pi}|\mathbf{x}-\boldsymbol{\xi}|^2\log|\mathbf{x}-\boldsymbol{\xi}| + R(\mathbf{x};\boldsymbol{\xi},\lambda). \tag{3.6b}$$

where R is a regular function at $\mathbf{x} = \boldsymbol{\xi}$. The constants $\boldsymbol{\alpha} = \{\alpha_1,\ldots,\alpha_N\}$ represent the strengths of singularity associated with each point constraint. The $(N+1)$ unknowns $(\boldsymbol{\alpha},\lambda_0)$ are determined by the $(N+1)$ conditions

$$\langle u_0, u_0\rangle = 1, \qquad u_0(\mathbf{x}_k) = 0, \quad k = 1,\ldots,N. \tag{3.7}$$

The numerical solution of (3.7) for a variety of patch configurations $\{\mathbf{x}_k\}_{k=1}^N$ is considered in Sec. 4. We now proceed to determine formulas for the corrections (λ_m, u_m) to this leading order

problem. The equation satisfied by u_m at order $\mathcal{O}(\nu^m)$ is

$$\Delta^2 u_m - \lambda_0 u_m = \lambda_m u_0 + \sum_{i=1}^{m-1} u_i \lambda_{m-i}\,, \quad \mathbf{x}\in\Omega\setminus\{\mathbf{x}_k\}_{k=1}^N\,; \qquad u_m = \frac{\partial u_m}{\partial n} = 0\,, \quad \mathbf{x}\in\partial\Omega\,, \tag{3.8a}$$

$$u_m \sim \mathbf{a}_{m-1,k}\cdot(\mathbf{x}-\mathbf{x}_k)\log|\mathbf{x}-\mathbf{x}_k| + [\mathbf{a}_{m-1,k}\cdot\mathcal{M}_k + \mathbf{a}_{m,k}]\cdot(\mathbf{x}-\mathbf{x}_k) + \cdots \quad \text{as} \quad \mathbf{x}\to\mathbf{x}_k\,, \tag{3.8b}$$

for $k=1,\ldots,N$. The sequence of problems (3.8) recursively determines the unknown vectors $\mathbf{a}_{m,k}$ for $m\geq 1$ and $k=1,\ldots,N$. In the case $m=1$ for example, the strength of singularity is prescribed as $\mathbf{a}_{0,k}=\nabla u_0|_{\mathbf{x}=\mathbf{x}_k}$ which uniquely determines u_1. Thereafter, matching the regular part of u_1 as $\mathbf{x}\to\mathbf{x}_k$ to the behavior (3.8*b*) provides a condition for $\mathbf{a}_{1,k}$. The recursive process continues, where matching the regular part at $\mathcal{O}(\nu^m)$ prescribes the strength of the singularity at $\mathcal{O}(\nu^{m+1})$ and so on. To incorporate the singularity structure (3.8*b*) into a solvability condition for the correction terms λ_m for $m\geq 1$, we first need to establish the following Lemma:

Lemma 1: *Let (u_0,λ_0) be an eigenpair of (3.4) with multiplicity one. Then, a necessary condition for the problem*

$$\Delta^2 u_m - \lambda_0 u_m = \lambda_m u_0 - f(\mathbf{x})\,, \quad \mathbf{x}\in\Omega\setminus\{\mathbf{x}_k\}_{k=1}^N\,; \qquad u_m = \frac{\partial u_m}{\partial n} = 0\,, \quad \mathbf{x}\in\partial\Omega\,; \tag{3.9a}$$

$$u_m \sim \mathbf{a}_{m-1,k}\cdot(\mathbf{x}-\mathbf{x}_k)\log|\mathbf{x}-\mathbf{x}_k|\,, \quad \text{as} \quad \mathbf{x}\to\mathbf{x}_k\,, \qquad k=1,\ldots,N, \tag{3.9b}$$

to have a solution is that λ_m satisfies

$$\lambda_m\,\langle u_0,u_0\rangle = \langle f,u_0\rangle + 4\pi\sum_{k=1}^N \mathbf{a}_{0,k}\cdot\mathbf{a}_{m-1,k}\,. \tag{3.10}$$

Here $\mathbf{a}_{0,k}=\nabla_{\mathbf{x}}u_0|_{\mathbf{x}=\mathbf{x}_k}$, and we have defined the inner product $\langle g,h\rangle\equiv\int_\Omega gh\,\mathrm{d}\mathbf{x}$.

Proof: To begin the proof, we consider the integral identity

$$\int_\Omega \left(u_0\Delta^2 u_m - u_m\Delta^2 u_0\right)\mathrm{d}\mathbf{x} = \int_{\partial\Omega}(u_0\partial_n(\Delta u_m) - \Delta u_m\partial_n u_0 - u_m\partial_n(\Delta u_0) + \Delta u_0\partial_n u_m)\mathrm{d}s$$

Upon multiplying (3.9*a*) by u_0 and integrating over $\Omega\setminus B_\sigma$, where $B_\sigma=\cup_{k=1}^N|\mathbf{x}-\mathbf{x}_k|\leq\sigma$, we obtain as $\sigma\to 0$

$$\begin{aligned}&\lambda_m\,\langle u_0,u_0\rangle - \langle f,u_0\rangle\\ &= \lim_{\sigma\to 0}\sum_{k=1}^N\int_{|\mathbf{x}-\mathbf{x}_k|=\sigma}(u_0\partial_n(\Delta u_m) - \Delta u_m\partial_n u_0 - u_m\partial_n(\Delta u_0) + \Delta u_0\partial_n u_m)\,\mathrm{d}s\,.\end{aligned} \tag{3.11}$$

To evaluate this integral in (3.11), we introduce a local polar coordinate system near $\mathbf{x}=\mathbf{x}_k$ where $r=|\mathbf{x}-\mathbf{x}_k|$ and $\mathbf{e}=(\cos\theta,\sin\theta)$. In addition, we note that $\partial_n=-\partial_r$ on $|\mathbf{x}-\mathbf{x}_k|=\sigma$. In terms of these quantities, we use the local behavior (3.9*b*) for u_m and from (3.5) $u_0\sim(\mathbf{a}_{0,k}\cdot\mathbf{e})\,r+\alpha_k\,r^2\log r$ as $r\to 0$ to calculate for $r\to 0$ that

$$\begin{aligned} u_m &\sim (\mathbf{a}_{m-1,k}\cdot\mathbf{e})\,r\log r, \qquad \partial_r u_m \sim (\mathbf{a}_{m-1,k}\cdot\mathbf{e})[\log r+1]\,,\\ \Delta u_m &\sim \frac{2}{r}(\mathbf{a}_{m-1,k}\cdot\mathbf{e})\,, \qquad \partial_r(\Delta u_m)\sim -\frac{2}{r^2}(\mathbf{a}_{m-1,k}\cdot\mathbf{e})\,;\\ u_0 &\sim (\mathbf{a}_{0,k}\cdot\mathbf{e})\,r+\alpha_k\,r^2\log r, \qquad \partial_r u_0\sim(\mathbf{a}_{0,k}\cdot\mathbf{e})+\alpha_k\,[2\log r+1]\,,\\ \Delta u_0 &\sim 4\alpha_k(\log r+1)\,, \qquad \partial_r(\Delta u_0)\sim\frac{4\alpha_k}{r}\,. \end{aligned}$$

The proof of the Lemma is concluded by substituting these quantities into (3.11), and then passing to the limit $\sigma \to 0$:

$$\lambda_m \langle u_0, u_0 \rangle - \langle f, u_0 \rangle = 4 \sum_{k=1}^{N} \int_0^{2\pi} (\mathbf{a}_{0,k} \cdot \mathbf{e})(\mathbf{a}_{m-1,k} \cdot \mathbf{e}) \, \mathrm{d}\theta = 4\pi \sum_{k=1}^{N} \mathbf{a}_{0,k} \cdot \mathbf{a}_{m-1,k} \,. \tag{3.12}$$

■

By applying this Lemma to (3.8) the coefficients λ_m in the expansion for the eigenvalue λ_ε are obtained as follows:

Principal Result 2: *Let (u_0, λ_0) be an eigenpair of (3.4) with multiplicity one, and assume $\sum_{k=1}^{N} |\nabla u_0(\mathbf{x}_k)|^2 \neq 0$, then an eigenvalue λ_ε of the perturbed problem (1.3) admits the expansion*

$$\lambda_\varepsilon = \lambda_0 + \sum_{m=1}^{M} \lambda_m \nu^m + \mathcal{O}(\nu^{M+1}) \,, \qquad \nu(\varepsilon) \equiv \frac{-1}{\log \varepsilon} \,, \tag{3.13a}$$

for any integer M and where λ_m for $m \geq 1$ are defined by

$$\lambda_1 = 4\pi \sum_{k=1}^{N} |\nabla u_0(\mathbf{x}_k)|^2 \,, \qquad \lambda_m = 4\pi \sum_{k=1}^{N} \nabla u_0(\mathbf{x}_k) \cdot \mathbf{a}_{m-1,k} - \sum_{i=1}^{m-1} \lambda_{m-i} \langle u_i, u_0 \rangle \,, \quad m \geq 2 \,. \tag{3.13b}$$

The vectors $\mathbf{a}_{m-1,k}$ for $m \geq 2$ and u_m for $m \geq 1$ are determined from (3.8).

The key feature of the analysis is that the difference $\lambda_\varepsilon - \lambda_0$ depends on the gradient of the base eigenfunction u_0 at each point of clamping. Crucially, this base eigenfunction u_0 is not determined by the problem in the absence of perturbing patches, but by the following problem with N additional point constraints:

$$\Delta^2 u_0 = \lambda_0 u_0 \,, \quad \mathbf{x} \in \Omega \setminus \{\mathbf{x}_k\}_{k=1}^{N} \,; \qquad u_0 = \frac{\partial u_0}{\partial n} = 0, \quad \mathbf{x} \in \partial\Omega \,; \qquad \int_\Omega u_0^2 \, \mathrm{d}\mathbf{x} = 1. \tag{3.14a}$$

$$u_0(\mathbf{x}_k) = 0 \,, \qquad u_0 \sim \alpha_k |\mathbf{x} - \mathbf{x}_k|^2 \log|\mathbf{x} - \mathbf{x}_k| + R_k(\mathbf{x}; \mathbf{x}_1, \ldots, \mathbf{x}_N, \lambda_0) + \cdots \qquad \mathbf{x} \to \mathbf{x}_k. \tag{3.14b}$$

This leading-order point constraint problem determines λ_0, and in terms of the solution we calculate $\mathbf{a}_{0,k} \equiv \nabla u_0|_{\mathbf{x}=\mathbf{x}_k}$ for $k = 1, \ldots, N$ from the regular part $R_k(\mathbf{x})$ of the limiting eigenfunction u_0. In the case where a clamping location $\mathbf{x}_k$ is a point at which u_0 has zero gradient, i.e. $\nabla u_0(\mathbf{x}_k) = 0$, then that location does not contribute to λ_1 in (3.12).

(a) Calculation of jump in eigenvalue

As the limiting problem does not correspond patch free eigenvalue problem for $(u^\star, \lambda^\star)$ satisfying

$$\Delta^2 u^\star = \lambda^\star u^\star, \quad \mathbf{x} \in \Omega; \qquad u^\star = \frac{\partial u^\star}{\partial n} = 0, \quad \mathbf{x} \in \partial\Omega; \qquad \int_\Omega u^{\star 2} \, \mathrm{d}\mathbf{x} = 1, \tag{3.15}$$

it is natural to investigate the magnitude of the discrepancy between the spectra of the two problems. For the jump in the eigenvalue $\lambda_0 - \lambda^\star$, we establish the following result:

Theorem 3: *Consider a simple eigenpair (u_0, λ_0) of the limiting problem (3.14) with local behavior (3.14b) as $\mathbf{x} \to \mathbf{x}_k$ for $k = 1, \ldots, N$ and a simple eigenpair $(u^\star, \lambda^\star)$ of the patch free problem (3.15). In the case where $\langle u_0, u^\star \rangle \neq 0$, then*

$$\lambda_0 - \lambda^\star = -\frac{8\pi}{\langle u_0, u^\star \rangle} \sum_{k=1}^{N} \alpha_k u^\star(\mathbf{x}_k), \qquad \langle u_0, u^\star \rangle = \int_\Omega u_0 u^\star \, \mathrm{d}\mathbf{x}. \tag{3.16}$$

Proof: To incorporate the singularity structure (3.14b) into the calculation of the jump in the eigenvalue, we integrate over the region $\Omega \setminus \cup_{k=1}^{N} B(\mathbf{x}_k, \sigma)$ where $B(\mathbf{x}_k, \sigma)$ is a ball of radius

σ centered at $\mathbf{x}_k \in \Omega$. Repeated integration by parts yields the following identity

$$(\lambda_0 - \lambda^\star)\int_\Omega u_0 u^\star \,\mathrm{d}\mathbf{x} = \lim_{\sigma\to 0}\int_{\Omega\setminus\cup_{k=1}^N B(\mathbf{x}_k,\sigma)} u^\star \Delta^2 u_0 - u_0\Delta^2 u^\star \,\mathrm{d}\mathbf{x}$$

$$= \sum_{k=1}^N \lim_{\sigma\to 0}\int_{\partial B(\mathbf{x}_k,\sigma)} u^\star \partial_n(\Delta u_0) - \partial_n u^\star \Delta u_0 - u_0\partial_n(\Delta u^\star) + \Delta u^\star \partial_n u_0 \,\mathrm{d}s \tag{3.17}$$

For each inclusion, we write $r = |\mathbf{x} - \mathbf{x}_k|$ and $(\mathbf{x} - \mathbf{x}_k) = r\,\mathbf{e} = r(\cos\theta, \sin\theta)$ so that the outward facing normal ∂_n of $\partial B(\mathbf{x}_k, \sigma)$ satisfies $\partial_n = -\partial_r$. From direct calculation, the local behavior (3.14*b*) yields the expressions

$$u_0 \sim \alpha_k r^2 \log r + r\,\mathbf{c}_k\cdot\mathbf{e} + \cdots, \qquad \partial_r u_0 \sim 2\alpha_k r\log r + \alpha_k r + \mathbf{c}_k\cdot\mathbf{e} + \cdots$$

$$\Delta u_0 \sim 4\alpha_k[\log r + 1] + \cdots, \qquad \partial_r(\Delta u_0) \sim \frac{4\alpha_k}{r} + \cdots.$$

where $\mathbf{c}_k = \nabla R_k|_{\mathbf{x}=\mathbf{x}_k}$. After substituting this local behavior into (3.17), together with $\partial_n = -\partial_r$, the limit as $\sigma \to 0$ is taken. Several terms tend to zero in this limit leaving the final result

$$(\lambda_0 - \lambda^\star)\langle u_0, u^\star\rangle = -\lim_{\sigma\to 0}\sum_{k=1}^N 2\pi\sigma\frac{4\alpha_k}{\sigma}u^\star(\mathbf{x}_k) = -8\pi\sum_{k=1}^N \alpha_k u^\star(\mathbf{x}_k) \tag{3.18}$$

In the case where $\langle u_0, u^\star\rangle \neq 0$, the result (3.16) is recovered. ■

The formula (3.18) can be interpreted as a generalization of the standard eigenfunction orthogonality relationship $\langle u_i, u_j\rangle = \delta_{ij}$ to the point constraint eigenvalue problem (3.4). This result also confirms the intuitive expectation that due to the common boundary conditions $u_0|_{\partial\Omega} = u^\star|_{\partial\Omega} = 0$, the contribution due to a particular puncture $\mathbf{x}_k$ vanishes as $\mathbf{x}_k \to \partial\Omega$. Moreover, the jump vanishes whenever the configuration $\{\mathbf{x}_k\}_{k=1}^N$ occupies the nodal set of the eigenfunction $u^\star(\mathbf{x})$.

A casual inspection of (3.18) might suggest that the puncture locations $\{\mathbf{x}_k\}_{k=1}^N$ which optimize the jump $(\lambda_0 - \lambda^\star)$ correspond to extrema of the unperturbed eigenfunction $u^\star$. However, the strengths of each singularity $\alpha_k = \alpha_k(\mathbf{x}_1, \ldots, \mathbf{x}_N)$ also carry a dependence on the puncture locations which is not known explicitly.

The lack of an explicit solution to the limiting problem (3.14) is a significant hinderance in understanding the dependence of λ_0 on the perforation pattern $\{\mathbf{x}_k\}_{k=1}^N$. Faced with this obstacle, we implement a numerical method which first seeks a numerical solution to problem (3.14) followed by iterative solution to obtain λ_0 from (3.7).

4. Numerical Investigation of the limiting Problem

In this section we numerically study the dependence of the principal eigenvalue λ_0 of the point constraint eigenvalue problem (3.14) on the number and location(s) of the patch centers $\{\mathbf{x}_k\}_{k=1}^N$. In particular, we focus on the determination of configurations $\{\mathbf{x}_k\}_{k=1}^N$ which give rise to the largest deviation from the eigenvalues of the patch free problem.

(a) Description of the Numerical Algorithm

The first step in our method exploits the linearity of the problem to separate the regular and singular portion of u_0 with the decomposition $u_0 = u_S + u_R$ where

$$u_S = \sum_{k=1}^N \alpha_k|\mathbf{x} - \mathbf{x}_k|^2\log|\mathbf{x} - \mathbf{x}_k|. \tag{4.1}$$

Substituting (4.1) into (3.14) yields that u_R satisfies

$$\Delta^2 u_R - \lambda_0 u_R = \lambda_0 u_S, \quad \mathbf{x} \in \Omega; \qquad u_R = -u_S, \quad \partial_n u_R = -\partial_n u_S, \quad \mathbf{x} \in \partial\Omega. \tag{4.2}$$

The $(N+1)$ unknowns $(\alpha_1, \ldots, \alpha_N, \lambda_0)$ are found by enforcing the point constraints $u_0(\mathbf{x}_k) = 0$ for $k = 1, \ldots, N$ together with the normalization condition $\alpha_1^2 + \cdots + \alpha_N^2 = 1$. This gives rise to the system of equations

$$\begin{bmatrix} u_S(\mathbf{x}_1) + u_R(\mathbf{x}_1) \\ \vdots \\ u_S(\mathbf{x}_N) + u_R(\mathbf{x}_N) \\ \alpha_1^2 + \cdots + \alpha_N^2 \end{bmatrix} = \begin{bmatrix} 0 \\ \vdots \\ 0 \\ 1 \end{bmatrix}. \tag{4.3}$$

which are solved by Newton-Raphson iterations for the singularity strengths $\boldsymbol{\alpha} = \{\alpha_1, \ldots, \alpha_N\}$ and eigenvalue $\lambda_0(\mathbf{x}_1, \ldots, \mathbf{x}_N)$. The normalization condition adopted in (4.3) is for numerical convenience only. Once a solution is obtained, it can be rescaled to satisfy $\langle u_0, u_0 \rangle = 1$, or any other normalization condition. Our numerical experiments are performed on the unit disk domain $\Omega = \{\mathbf{x} \in \mathbb{R}^2 \mid |\mathbf{x}| \leq 1\}$ and employ a finite difference method to discretize (4.2) in polar co-ordinates (r, θ) with a uniform polar mesh consisting of $N_r \times N_\theta$ points.

To track the first eigenvalue as the isolated points $\{\mathbf{x}_k\}_{k=1}^N$ vary, we utilized the parameter continuation feature of `Bertini` which has been successfully applied to compute bifurcation branches in related problems [21–24]. The fourth order nature of (4.2) means that the condition number on the Jacobian matrix of the discretized system increases rapidly as (N_r, N_θ) increases. To maintain convergence of the numerical scheme and accurately track the paths, we have used adaptive higher precision arithmetic [6,7]. In Table 1 we demonstrate second order convergence of our numerical scheme on an exactly solvable test case, once adaptive precision is utilized.

	Double precision		Multiple precision	
(N_r, N_θ)	$\max f_i$	Order	$\max f_i$	Order
$(5, 32)$	6.08×10^{-3}	–	6.08×10^{-3}	–
$(10, 64)$	1.58×10^{-3}	1.94	1.58×10^{-3}	1.94
$(20, 128)$	4.00×10^{-4}	1.99	4.00×10^{-4}	1.99
$(40, 256)$	1.00×10^{-4}	2.00	1.00×10^{-4}	2.00
$(80, 512)$	2.52×10^{-5}	1.99	2.52×10^{-5}	1.99
$(160, 1024)$	1.08×10^{-5}	1.22	6.31×10^{-5}	2.00
$(320, 2048)$	7.68×10^{-5}	−2.83	1.58×10^{-5}	2.01

Table 1. Convergence of the numerical scheme for system $\Delta^2 u = \frac{45}{r^4} u$, with analytical solution $u = r^4 \cos\theta$. As (N_r, N_θ) increases, adaptive precision is required to maintain second order convergence order of the scheme.

At this point, we briefly review closed form solutions of the patch free (1.4) and punctured (3.14) problems. The factorization $\Delta^2 - \mu^4 = (\Delta - \mu^2)(\Delta + \mu^2) = 0$ indicates that for the unit disc scenario, the eigenfunctions take the form

$$\phi_{m,n}(r, \theta) = e^{im\theta}\{J_m(\mu_{m,n} r), Y_m(\mu_{m,n} r), K_m(\mu_{m,n} r), I_m(\mu_{m,n} r)\}, \qquad \mu_{m,n} = \lambda_{m,n}^{1/4}, \tag{4.4}$$

where $m = 0, \pm 1, \pm 2, \ldots$ and $J_m(z), Y_m(z), I_m(z)$ and $K_m(z)$ are the standard Bessel functions. In the patch free problem (1.4), the smooth eigenfunctions satisfying $u^\star = \partial_r u^\star = 0$ on $r = 1$ are

$$\phi_{mn}^\star = e^{im\theta}\left[J_m(\mu_{m,n}^\star r) - \frac{J_m(\mu_{m,n}^\star)}{I_m(\mu_{m,n}^\star)} I_m(\mu_{m,n}^\star r)\right], \tag{4.5a}$$

and the eigenvalues $\mu^\star_{m,n}$ solve the nonlinear equation

$$J'_m(\mu^\star_{m,n})I_m(\mu^\star_{m,n}) = I'_m(\mu^\star_{m,n})J_m(\mu^\star_{m,n}). \tag{4.5b}$$

The first four eigenvalues $\lambda^\star_{m,n} = (\mu^\star_{m,n})^4$ are found from numerical solution of (4.5*b*) to be

$$\lambda^\star_{0,0} = 104.4, \qquad \lambda^\star_{1,0} = 452.0, \qquad \lambda^\star_{2,0} = 1216.4, \qquad \lambda^\star_{0,1} = 1581.7, \tag{4.6}$$

and in Fig. 3, the associated eigenfunctions are plotted.

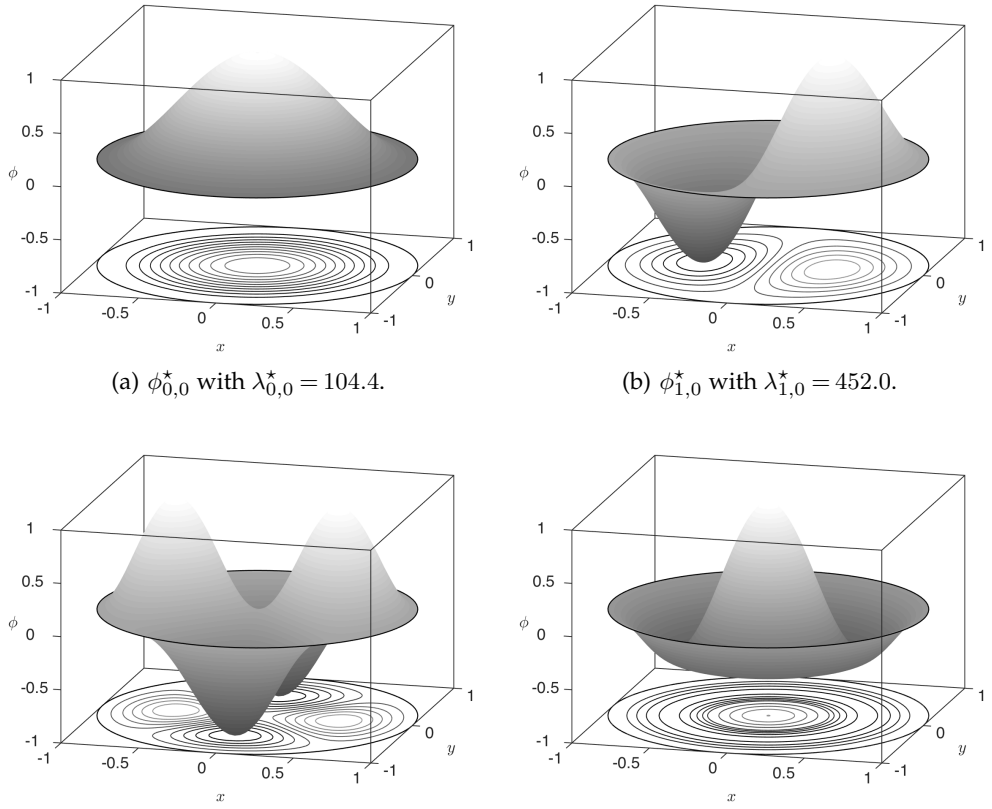

(a) $\phi^\star_{0,0}$ with $\lambda^\star_{0,0} = 104.4$. (b) $\phi^\star_{1,0}$ with $\lambda^\star_{1,0} = 452.0$.

(c) $\phi^\star_{2,0}$ with $\lambda^\star_{2,0} = 1216.4$. (d) $\phi^\star_{0,1}$ with $\lambda^\star_{0,1} = 1581.7$.

Figure 3. The first four eigenfunctions of the bi-Laplacian (1.4) on the unit disc with no punctures and clamped boundary conditions at $r = 1$.

In the punctured case, we can develop a closed form solution of (3.14) for $N = 1$ and $\mathbf{x}_0 = (0, 0)$. The radially symmetric eigenfunctions ($m = 0$) of (3.14) are spanned by (4.4) and those satisfying $u_0(0) = 0$ and $u_0(1) = \partial_r u_0(1) = 0$ are

$$u_0(r) = A\Big[J_0(\mu_{0,n}r) - I_0(\mu_{0,n}r) - \Big(\frac{J_0(\mu_{0,n}) - I_0(\mu_{0,n})}{\frac{2}{\pi}K_0(\mu_{0,n}) + Y_0(\mu_{0,n})}\Big)\Big(\frac{2}{\pi}K_0(\mu_{0,n}r) + Y_0(\mu_{0,n}r)\Big)\Big], \tag{4.7a}$$

where the eigenvalues $\lambda_{0,n} = \mu^4_{0,n}$ are determined by the relationship

$$\big(J_0(\mu_{0,n}) - I_0(\mu_{0,n})\big)\Big(\frac{2}{\pi}K_1(\mu_{0,n}) + Y_1(\mu_{0,n})\Big) = \big(J_1(\mu_{0,n}) + I_1(\mu_{0,n})\big)\Big(\frac{2}{\pi}K_0(\mu_{0,n}) + Y_0(\mu_{0,n})\Big). \tag{4.7b}$$

Here A is a constant set by the normalization condition $\langle u_0, u_0 \rangle = 1$. The smallest positive root of (4.7*b*) is

$$\lambda_{0,0} = 516.9609. \tag{4.8}$$

This exact solution provides a benchmark against which the efficacy of our numerical method can be verified (see Table. 2).

(N_r, N_θ)	The minimum eigenvalue	Error (Relative)
$(20, 5)$	496.3	20.7 (4.02%)
$(40, 5)$	510.9	6.07 (1.17%)
$(80, 5)$	515.4	1.55 (0.30%)
$(160, 5)$	516.5	0.39 (0.08%)

Table 2. Convergence of the numerical scheme to the first eigenvalue of (3.14) in the case $\mathbf{x}_0 = (0, 0)$. The exact value, provided by the closed form solution, is given in (4.8).

(b) Results

Numerical determination of the configurations $\{\mathbf{x}_k\}_{k=1}^N$ optimizing $\lambda_0(\mathbf{x}_1, \ldots, \mathbf{x}_N)$ is challenging on account of several factors. Principally, for any given configuration, λ_0 is determined by solving a nonlinear system of equations, each evaluation of which requires solving the fourth order PDE (4.2). Numerical optimization of this objective function is therefore computationally intensive, particularly as the number of unknown increases. As an initial step in analyzing the optimizing locations $\{\mathbf{x}_k\}_{k=1}^N$, we seek extrema over ring configurations to reduce the number of unknowns over which to optimize. For punctures periodically spaced on a ring of radius r, the centers are given explicitly by

$$\begin{pmatrix} \text{One Ring} \\ \text{Pattern} \end{pmatrix} \qquad \mathbf{x}_k = r\Big(\cos\frac{2\pi k}{N}, \sin\frac{2\pi k}{N}\Big), \qquad k = 1, \ldots, N, \tag{4.9}$$

which leaves a single variable r over which to optimize.

In the case $N = 1$, we examine the dependence of the first two eigenvalues on r. In Fig. 4(a), the first two eigenvalues are seen to converge to $\lambda^\star_{0,0} = 104.4$ and $\lambda^\star_{1,0} = 452.0$ as $r \to 1$, in agreement with (3.18). The eigenfunctions associated with the lowest eigenvalue makes a connection between the second (mode 1) eigenfunction $\phi^\star_{1,0}$ and the radially symmetric eigenfunction $\phi^\star_{0,0}$ of the patch free problem (1.4), as $r \to 1$. In an opposite fashion, the eigenfunctions associated with the second eigenvalue, are continuously deformed from the point constraint problem (4.7) to the second (mode 1) eigenfunction $\phi^\star_{1,0}$ of the patch free problem.

In Fig. 5(a), the principal eigenvalue $\lambda_0(r)$ is plotted against r for the case $N = 2$ and a unique global maximum is observed at (r_c, λ_c). The open circles represent the eigenvalues of the unperturbed problem (1.4), and in agreement with (3.18), the curve $\lambda_0(r)$ tends to this value as $r \to 1$. As $r \to 0$ we see that $\lambda_0(r) \to \lambda_{0,0}$ where $\lambda_{0,0}$ is the exact value obtained in (4.8).

Table 4 displays the numerically computed maximizing ring radius along with the associated maximum principal eigenvalue.

N	1	2	3	4	5	6	7	8
λ_c	452.1	732.6	1263.8	1582.3	1582.4	1582.5	1582.5	1582.5
r_c	0.0	0.23	0.35	0.38	0.38	0.38	0.38	0.38

Table 3. (Single Ring) Maximum first eigenvalue λ_c for an arrangement of N periodically spaced punctures on a single ring of radius r_c.

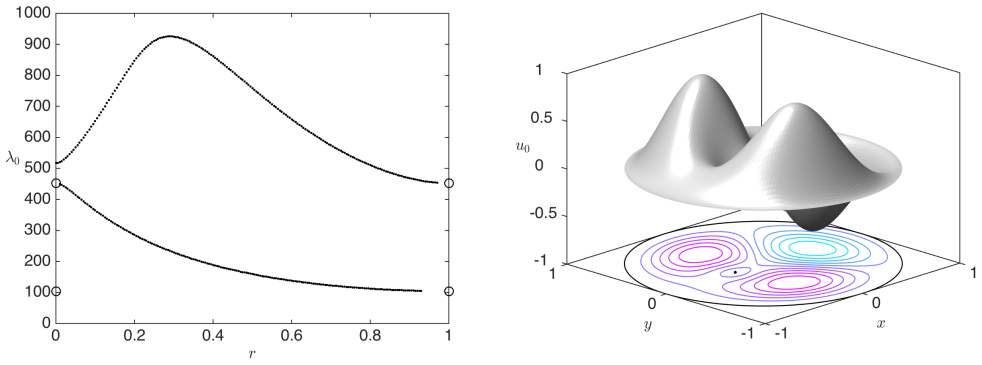

(a) λ_0 against r for $N = 1$. (b) Second Eigenfunction $u_0(\mathbf{x}; \lambda_c)$ for $N = 1$

Figure 4. Numerical solution of (3.14) for $N = 1$ perforation. Left Panel: Plot of $\lambda_0(r)$ against r. The lowest eigenvalue behaves monotonically while the second has a pronounced maximum at (r_c, λ_c). Open circles represent eigenvalues of the patch free problem (1.4). Right Panel: The eigenfunction $u_0(\mathbf{x}; \lambda_c)$ corresponding to the maximum of the second eigenvalue.

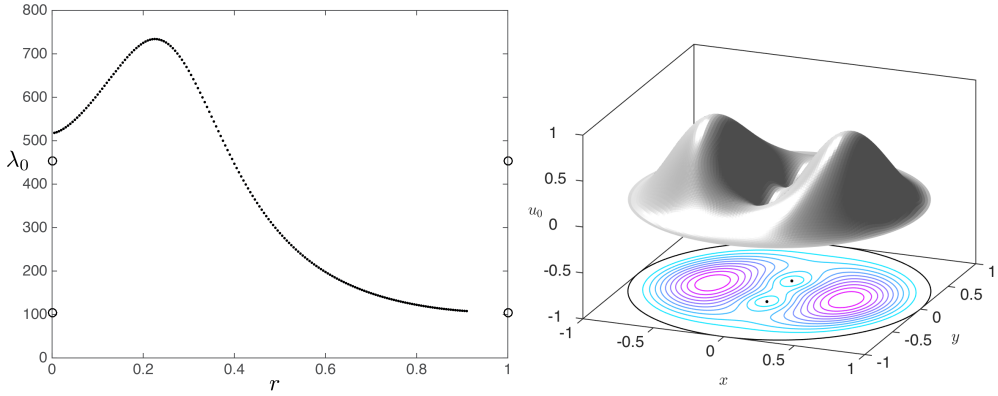

(a) λ_0 against r for $N = 2$. (b) Eigenfunction $u_0(\mathbf{x}; \lambda_c)$ for $N = 2$

Figure 5. Numerical solution of (3.14) for $N = 2$ perforations. Left Panel: Plot of $\lambda_0(r)$ against ring radius r with a pronounced maximum at (r_c, λ_c). Open circles represent eigenvalues of the corresponding problem with no patches (1.4). Right Panel: The eigenfunction $u_0(\mathbf{x}; \lambda_c)$ corresponding to the maximum of the second eigenvalue.

For a single ring with N punctures, we observe $\lim_{N\to\infty}(\lambda_c, r_c) \approx (1582.5, 0.38)$. The extrema calculated in Table 4 are based on the particular ring based anzatz (4.9), are not necessarily indicative of a globally optimal pattern.

$$\left(\begin{array}{c}\text{One Ring with}\\ \text{center Puncture}\end{array}\right) \qquad \mathbf{x}_k = r\left(\cos\frac{2\pi k}{N-1}, \sin\frac{2\pi k}{N-1}\right), \qquad k = 1, \ldots, N-1; \qquad \mathbf{x}_N = (0,0); \tag{4.10}$$

In table 4, we observe that a ring with a puncture at the center generates a larger maximum eigenvalue over a single ring case for $N \geq 5$. As with the single ring case (4.9), the maximum eigenvalue saturates as N increases with limiting behavior $(r_c, \lambda_c) \sim (0.50, 3838.4)$ as $N \to \infty$.

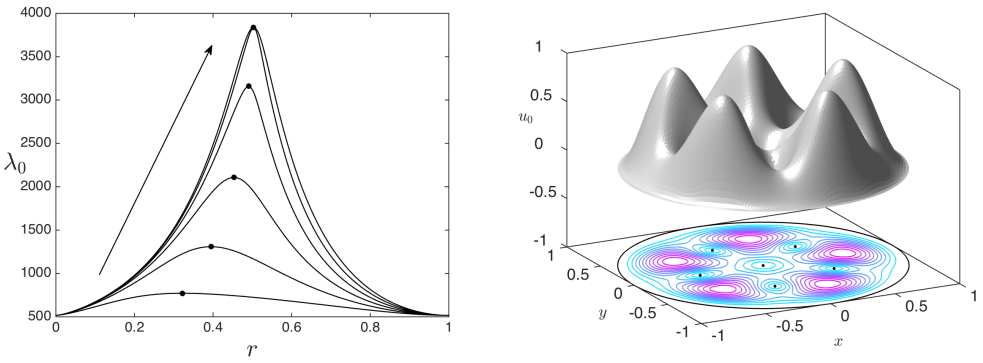

(a) λ_0 against r. (b) Eigenfunction for $N = 6$.

Figure 6. (Single Ring with center puncture) Puncture configuration (4.10). Left: lowest eigenvalue $\lambda_{0,0}(r)$ for configurations (4.10) with a puncture at $(0,0)$ and $(N-1)$ periodically spaced punctures on a ring of radius r. Curves plotted for $N = 3, \ldots, 8$ with arrow indicating direction of increasing N. Right: The eigenfunction associated with the maximum eigenvalue for $N = 6$.

N	3	4	5	6	7	8
λ_c	771.5	1308.5	2106.6	3158.7	3836.0	3838.3
r_c	0.32	0.40	0.45	0.49	0.50	0.50

Table 4. (Single Ring with center puncture) Maximum of the first eigenvalue λ_c for an arrangement of N punctures with one fixed at $(0,0)$ and $N-1$ periodically spaced punctures on a single ring of radius r_c.

This limiting behavior suggests that additional points should be placed on a new ring in order to achieve large values of λ_c. The family of two ring puncture patterns is given by

$$\left(\begin{array}{c}\text{Two Ring}\\ \text{Pattern}\end{array}\right) \quad \begin{aligned} \mathbf{x}_k &= r_1\Big(\cos\frac{2\pi k}{N_1}, \sin\frac{2\pi k}{N_1}\Big), && k = 1, \ldots, N_1;\\ \mathbf{x}_k &= r_2\Big(\cos\frac{2\pi(k-N_1)}{N_2}, \sin\frac{2\pi(k-N_1)}{N_2}\Big), && k - N_1 = 1, \ldots, N_2, \end{aligned} \tag{4.11}$$

for $r_1 > r_2$ and $N_1 \geq N_2$. The system for λ_0 is solved over all $0 < r_2 < r_1 < 1$ and the maximum value recorded (cf Fig. 7). In Table 5, the maximum first eigenvalue is displayed for a range of two ring configurations.

N	6		7		8			9		
(N_1, N_2)	$(3,3)$	$(4,2)$	$(4,3)$	$(5,2)$	$(4,4)$	$(5,3)$	$(6,2)$	$(5,4)$	$(6,3)$	$(7,2)$
λ_c	1388.9	2174.6	2447.3	3325.5	2327.8	3449.0	3458.3	3688.0	4756.2	4584.7
r_{1c}	0.50	0.48	0.56	0.52	0.57	0.55	0.51	0.56	0.54	0.61
r_{2c}	0.26	0.23	0.32	0.26	0.35	0.29	0.14	0.49	0.22	0.22

Table 5. Maximum values for the first eigenvalue over two ring patterns (4.11).

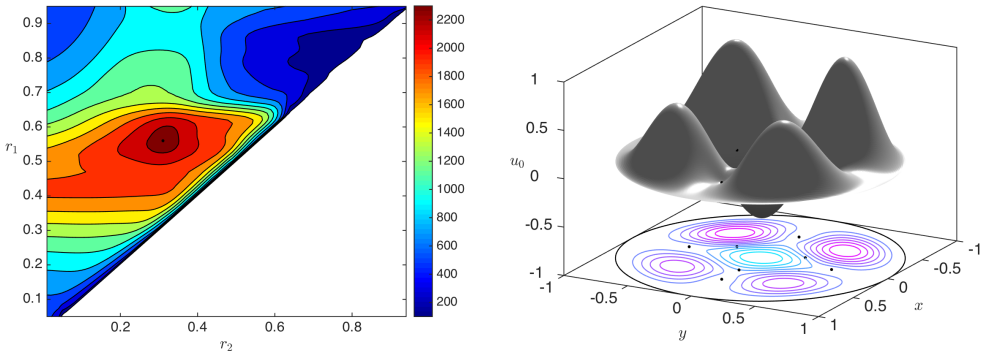

Figure 7. Two ring pattern (4.11) with $N_1 = 4$ and $N_2 = 3$. Left Panel: The landscape of eigenvalues for $0.05 < r_2 < r_1 < 0.95$ with the global max at $(r_{1c}, r_{2c}) = (0.56, 0.32)$. Right panel: The eigenfunction corresponding to the eigenvalue $\lambda_c = 2447.3$.

For $N = 1, \ldots, 9$, we display in Fig. 8 the configurations of patch centers which generate the local maximum first eigenvalue over the patterning schemes with one ring (4.9), one ring with a center puncture (4.10) and two rings (4.11).

5. Conclusion

In this paper, we have studied the problem for the modes of vibration of a thin elastic plate with a collection of clamped patches. As the patch radius shrinks to zero, the limiting problem is *not* the patch free problem, but a point constraint eigenvalue problem. The contribution of the present work is three fold. First, we have obtained detailed information on this limiting behavior in the form of an asymptotic expansion in the limit of small patch radius. Second, exact expressions for the jump between the point constraint eigenvalues (1.8) and patch free eigenvalues (1.4) were obtained in (3.18). The third contribution of this work is a numerical study on the dependence of the vibrational modes with respect to the number and location of clamping points.

The numerical study of Sec. 4 indicates that the vibrational characteristics of the plate depend sensitively on the clamping configuration $\{\mathbf{x}_k\}_{k=1}^N$. The introduction of small clamped patches can be seen (cf. Fig. 6) to change the basal frequency by almost an order of magnitude if the patches are centered at particular locations. This naturally gives rise to the question of which configurations induce the largest deviation form the patch free problem. For the cases $N = 1, \ldots, 9$, we have numerically calculated (locally) optimal configurations for disk geometry.

There are many avenues of future investigation which arise from this study. Prominent amongst them is the question of determining the patch centers $\{\mathbf{x}_k\}_{k=1}^N$ which maximize the first eigenvalue of (1.8) for larger values of N and on non-radially symmetric domains. Analytical progress towards this goal can be made by establishing detailed knowledge of the bi-Laplacian Helmoltz Green's function

$$-\Delta^2 G + \lambda G = -\delta(\mathbf{x} - \mathbf{x}_0), \quad \mathbf{x} \in \Omega; \qquad G = \frac{\partial G}{\partial n} = 0, \quad \mathbf{x} \in \partial\Omega; \tag{5.1a}$$

$$G(\mathbf{x}; \mathbf{x}_0, \lambda) = \frac{1}{8\pi} |\mathbf{x} - \mathbf{x}_0|^2 \log |\mathbf{x} - \mathbf{x}_0| + R(\mathbf{x}; \mathbf{x}_0, \lambda). \tag{5.1b}$$

Aside from the symmetric case (cf. (4.7)) where Ω is a disk and $\mathbf{x}_0 = (0, 0)$, we know of no closed form exact solutions to (3.6). Such a solution would be very useful in determining optimizing configurations of clamping points $\{\mathbf{x}_k\}_{k=1}^N$. Furthermore, such information would be very useful for investigating the nature of globally optimal clamping patterns.

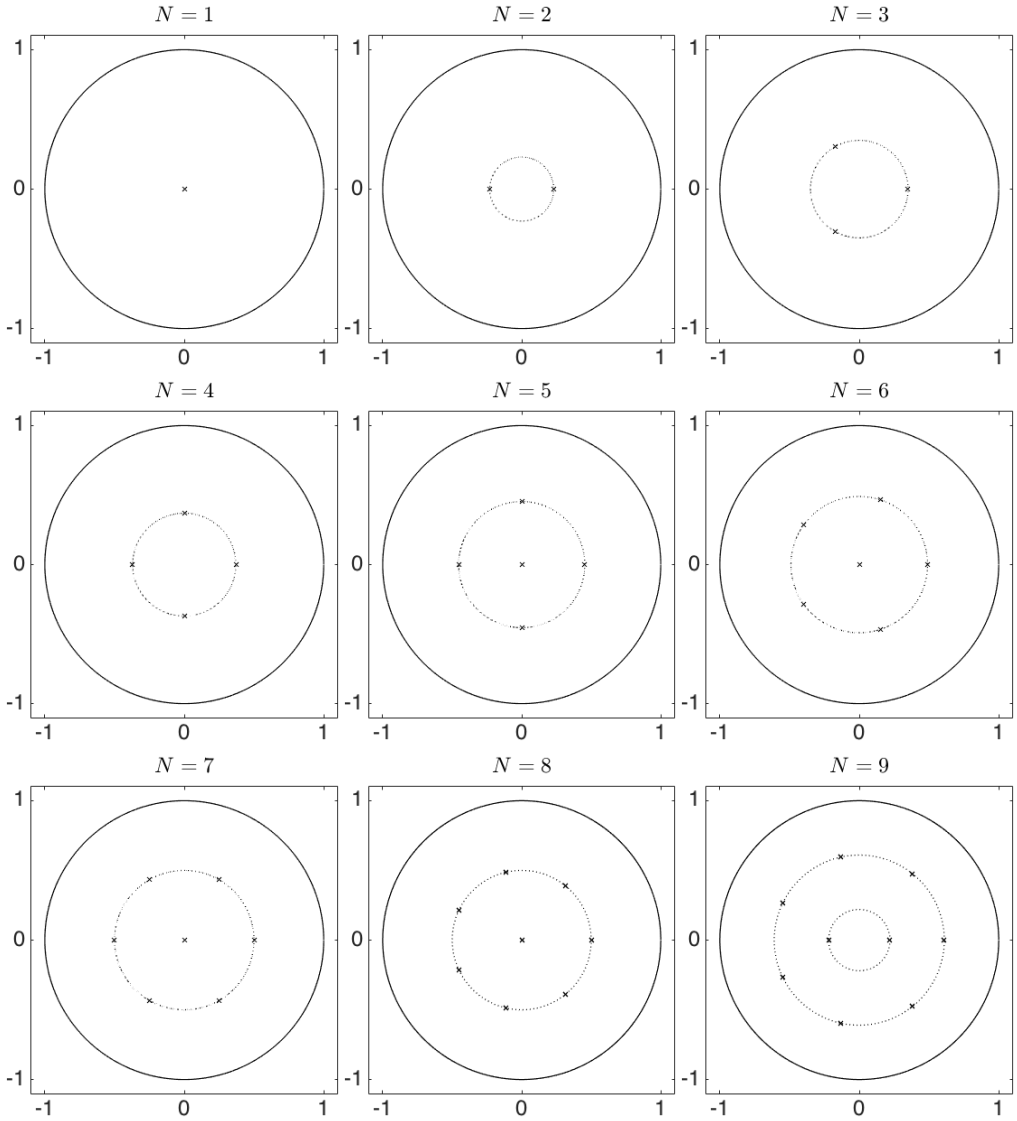

Figure 8. Puncture configurations which maximize the first eigenvalues of (3.14) over configurations (4.9), (4.10) and (4.11).

In scenarios where a numerical solution of the full PDE (4.2) is required for each solution of the eigenvalue problem (4.3), it is highly desirable to have an accurate and efficient solution technique which is adaptable to a variety of geometries. An integral equation approach seems well suited to accomplish this goal (cf. [26]).

This paper has largely focussed on the dependence of the fundamental eigenfunction and eigenvalue on the perforation configuration. We also expect a significant effect on localization in higher modes, as seen in [16] for the case of a rectangular domain and $N = 1$. A interesting problem would study this phenomenon and determine a theory for the placement of punctures to achieve a desired localization pattern.

Acknowledgements. We acknowledge the assistance of the Notre Dame Center for Research Computing (CRC)

Authors' Contribution. AEL conceived the problem, performed analysis and wrote manuscript. WH and AJS performed numerical simulations with `Bertini` software package [4,5].

Ethics Statement. This research poses no ethical considerations.

Data accessibility statement. This work does not involve any experimental data.

Competing Interests Statement. We have no competing interests.

Funding. AEL acknowledges support from the National Science Foundation under Grant DMS-1516753. WH has been supported by the Mathematical Biosciences Institute and the National Science Foundation under Grant DMS-0931642. AJS acknowledges support from the National Science Foundation under Grant ACI-1440607.

References

1. Carlos J. S. Alves and Pedro R. S. Antunes.
The method of fundamental solutions applied to the calculation of eigensolutions for 2d plates.
International Journal for Numerical Methods in Engineering, 77(2):177–194, 2009.
2. I.V. Andrianov, V.V. Danishevs'kyy, and A.L. Kalamkarov.
Asymptotic analysis of perforated plates and membranes. part 2: Static and dynamic problems for large holes.
International Journal of Solids and Structures, 49(2):311–317, 2012.
3. Noureddine Atalla and Franck Sgard.
Modeling of perforated plates and screens using rigid frame porous models.
Journal of Sound and Vibration, 303(1-2):195–208, 2007.
4. D. J. Bates, J. D. Hauenstein, A. J. Sommese, and C. W. Wampler.
Bertini: Software for numerical algebraic geometry.
Available at `bertini.nd.edu`.
5. D. J. Bates, J. D. Hauenstein, A. J. Sommese, and C. W. Wampler.
Numerically solving polynomial systems with Bertini.
SIAM, Singapore, 2013.
6. D. J. Bates, J. D. Hauenstein, A. J. Sommese, and C. W. Wampler, II.
Adaptive multiprecision path tracking.
SIAM J. Numer. Anal., 46(2):722–746, 2008.
7. D. J. Bates, J. D. Hauenstein, A. J. Sommese, and C. W. Wampler, II.
Stepsize control for path tracking.
In *Interactions of classical and numerical algebraic geometry*, volume 496 of *Contemp. Math.*, pages 21–31. Amer. Math. Soc., Providence, RI, 2009.
8. B. M. Brown, E. B. Davies, P. K. Jimack, and M. D. Mihajlović.
A numerical investigation of the solution of a class of fourth order eigenvalue problems.
Proceeding of the Royal Society A: Mathematical Physical & Engineering Sciences, 456(1998):1505–1521, 2000.
9. K.A. Burgemeister and C.H. Hansen.
Calculating resonance frequencies of perforated panels.
Journal of Sound and Vibration, 196(4):387–399, 1996.
10. A. Campbell and S.A. Nazarov.
Asymptotics of eigenvalues of a plate with small clamped zone.
Positivity, 5:275–295, 2001.
11. Gilles Chardon and Laurent Daudet.
Low-complexity computation of plate eigenmodes with vekua approximations and the method of particular solutions.
Computational Mechanics, 52(5):983–992, 2013.
12. C. Coffman.

On the structure of solutions $\Delta^2 u = \lambda u$ which satisfy the clamped plate conditions on a right angle.
SIAM Journal on Mathematical Analysis, 13(5):746–757, 1982.

13. C. V. Coffman, R. J. Duffin, and D. H. Shaffer.
The fundamental mode of vibration of a clamped annular plate is not of one sign.
Constructive Approaches to Mathematical Models (Proc. Conf. in honor of R. J. Duffin, Pittsburgh, PA.), pages 267–277, 1979.
14. Charles V Coffman and Richard J Duffin.
On the fundamental eigenfunctions of a clamped punctured disk.
Advances in Applied Mathematics, 13(2):142–151, 1992.
15. Lawrence C. Evans.
Partial Differential Equations: Second Edition.
American Mathematical Society, 2010.
16. Marcel Filoche and Svitlana Mayboroda.
Strong localization induced by one clamped point in thin plate vibrations.
Phys. Rev. Lett., 103:254301, Dec 2009.
17. M. Flucher.
Approximation of dirichlet eigenvalues on domains with small holes.
Journal of Mathematical Analysis and Applications, 193(1):169–199, 1995.
18. Filippo Gazzola, Hans-Christoph Grunau, and Guido Sweers.
Polyharmonic Boundary Value Problems.
Springer, 2010.
19. David Gilbarg and Neil S. Trudinger.
Elliptic Partial Differential Equations of Second Order.
Springer, 1998.
20. Hans-Christoph Grunau and Guido Sweers.
In any dimension a "clamped plate" with a uniform weight may change sign.
Nonlinear Analysis: Theory, Methods and Applications, 97(0):119 – 124, 2014.
21. W. Hao, J. D. Hauenstein, B. Hu, T. McCoy, and A. J. Sommese.
Computing steady-state solutions for a free boundary problem modeling tumor growth by Stokes equation.
J. Comput. Appl. Math., 237(1):326–334, 2013.
22. W. Hao, J. D. Hauenstein, Bei Hu, Yuan Liu, A. J. Sommese, and Yong-Tao Zhang.
Bifurcation for a free boundary problem modeling the growth of a tumor with a necrotic core.
Nonlinear Anal. Real World Appl., 13(2):694–709, 2012.
23. W. Hao, J. D. Hauenstein, Bei Hu, Yuan Liu, A. J. Sommese, and Yong-Tao Zhang.
Continuation along bifurcation branches for a tumor model with a necrotic core.
J. Sci. Comput., 53(2):395–413, 2012.
24. W. Hao, J. D. Hauenstein, Bei Hu, and A. J. Sommese.
A three-dimensional steady-state tumor system.
Appl. Math. Comput., 218(6):2661–2669, 2011.
25. L. Jaouen and F.-X. Bécot.
Acoustical characterization of perforated facings.
The Journal of the Acoustical Society of America, 129(3):1400–1406, 2011.
26. Shidong Jiang, Mary Catherine A. Kropinski, and Bryan D. Quaife.
Second kind integral equation formulation for the modified biharmonic equation and its applications.
Journal of Computational Physics, 249(0):113 – 126, 2013.
27. T. Kolokolnikov, M. S. Titcombe, and M. J. Ward.
Optimizing the fundamental neumann eigenvalue for the laplacian in a domain with small traps.
European Journal of Applied Mathematics, 16:161–200, 4 2005.
28. K. Krishnakumar and G. Venkatarathnam.
Transient testing of perforated plate matrix heat exchangers.
Cryogenics, 43(2):101–109, 2003.
29. M.C. Kropinski, A.E. Lindsay, and M.J. Ward.
Asymptotic analysis of localized solutions to some linear and nonlinear biharmonic eigenvalue problems.

Studies in Appl. Math., 126(4):347–408, 2011.
30. W. M. Lee and J. T. Chen.
Free vibration analysis of circular plates with multiple circular holes using indirect biem and addition theorem.
J. Appl. Mechanics, 78(1), 2010.
31. A. E. Lindsay, M. J. Ward, and T. Kolokolnikov.
The transition to point constraint in a mixed biharmonic eigenvalue problem.
SIAM Journal on Applied Mathematics, 75(3):1193–1224, 2015.
32. Michael J. Nilles, Myron E. Calkins, Michael L. Dingus, and John B. Hendricks.
Heat transfer and flow friction in perforated plate heat exchangers.
Experimental Thermal and Fluid Science, 10(2):238–247, 1995.
Aerospace Heat Exchanger Technology.
33. Shin Ozawa.
Singular variation of domains and eigenvalues of the laplacian.
Duke Mathematical Journal, 48(4):767–778, 12 1981.
34. J. N. Reddy.
Theory and Analysis of Plates and Shells.
CRC Press, Taylor and Francis, 2007.
35. G. Sweers.
When is the first eigenfunction for the clamped plate equation of fixed sign?
Electronic J. Differ. Equ. Conf. Southwest Texas State Univ., San Marcos, Texas, 6:285–296, 2001.
36. M. Titcombe, M.J. Ward, and M.C. Kropinski.
A hybrid asymptotic-numerical method for low reynolds number flow past an asymmetric cylindrical body.
Studies in Appl. Math., 105(2):165–195, 2000.
37. G. Venkatarathnam.
Effectiveness-n_{tu} relationship in perforated plate matrix heat exchangers.
Cryogenics, 36(4):235–241, 1996.
38. Chunqi Wang, Li Cheng, Jie Pan, and Ganghua Yu.
Sound absorption of a micro-perforated panel backed by an irregular-shaped cavity.
The Journal of the Acoustical Society of America, 127(1):238–246, 2010.
39. M. Ward, W. Heshaw, and J. Keller.
Summing logarithmic expansions for singularly perturbed eigenvalue problems.
SIAM Journal on Applied Mathematics, 53(3):799–828, 1993.
40. M. Ward and J. Keller.
Strong localized perturbations of eigenvalue problems.
SIAM Journal on Applied Mathematics, 53(3):770–798, 1993.